Revisiting the catalytic activity of a doped $SrFeO_3$ for water pollutants removal: Effect of light and temperature

Maria Laura Tummino [a], Enzo Laurenti [a,*], Francesca Deganello [b], Alessandra Bianco Prevot [a], Giuliana Magnacca [a,c]

[a] *Università di Torino, Dipartimento di Chimica, Via P. Giuria 7, 10125 Torino, Italy*
[b] *Istituto per lo Studio dei Materiali Nanostrutturati (ISMN) — Consiglio Nazionale delle Ricerche (CNR), UOS Palermo, Via Ugo La Malfa 153, 90146, Palermo, Italy*
[c] *NIS and INSTM Reference Centre, Via P. Giuria 7, 10125 Torino, Italy*
[*] Corresponding author. *E-mail address:* enzo.laurenti@unito.it (E. Laurenti).

Abstract

A $Sr_{0.85}Ce_{0.15}FeO_{3-}$ perovskite-type mixed oxide was prepared by solution combustion synthesis from citric acid and carefully characterized for the structure by X-ray diffraction coupled with Rietveld analy-sis, for the microstructure/morphology by HRTEM and SEM, for texture by N_2 uptake at low temperature, for surface charge by ζ potential measurements and for reactive species by Electron Paramagnetic Reso- nance (EPR). Photocatalytic activity was tested in the presence of simulated solar light towards Orange II and Rhodamine B as model pollutants. Despite this compound is known as photocatalyst, a good reac-tivity was evidenced in the 55–80 °C temperature range without light irradiation, indicating that it canwork as well in the dark after thermal-activation. Therefore, experimental data obtained in this work suggest to carefully reconsidering the role of this mixed oxide as photocatalyst. EPR spin-trapping testsallowed to deepen the aspects related to reactive species generated by $Sr_{0.85}Ce_{0.15}FeO_{3-}$, revealing that the temperature increase promotes hydroxyl radicals and singlet oxygen production. Furthermore, an interesting selectivity towards the degradation of different dyes was found.

Keywords: Doped-strontium ferratePerovskite, Thermal activationPhotocatalysis Water remediation

1. Introduction

Perovskite-type materials are mixed oxides with general formula ABO_3. This class of compounds is very versatile since its properties can be easily tailored either by changing the chemi-cal composition, by introducing dopant elements or by modifying synthesis methods.

New interesting applications of perovskite materials containing strontium in the A–site are recently emerging. For example it has been demonstrated that $SrTiO_3$ is able to promote the degradation of tetracycline [1] and enhance hydrogen production by means of water splitting [2,3].

Herein, a doped strontium ferrate perovskite is studied. The most relevant feature of strontium ferrate ($SrFeO_{3-}$) is that the main oxidation state of iron at the B-site is IV, which is quite uncommon with respect to the usual Fe^{3+}, mostly found in other iron perovskites [4,5]. Doped strontium ferrate perovskites can be applied in many contexts, as sensors, as catalysts for energy devices and in the controlled oxidation of pollutants [5–8] and, in most of these cases, high temperatures are necessary to exploit their catalytic activity. Undoped strontium ferrate perovskites found a place also in water remediation field since they were used as photocatalysts irradiated by both UV and visible light. Indeed, it was shown that they are able to induce the degradation of nitroben- zene [7], methylene blue [9], methylorange [10], phenol [11], bisphenol A and Acid Orange 8 [12]. Although the different exper- imental conditions reported do not allow a direct comparison, the results evidenced degradation levels ranging from 35% in 24 h for methylene blue to 99% in 6 h for nitrobenzene and the complete abatement of Acid Orange 8 in 1 h.

Bandgap energy values reported in literature for $SrFeO_3$ compounds are comprised between 1.80 [9] and 3.75 eV [7] and are considered determining parameters for their photocatalytic properties. On the other hand, as already mentioned, $SrFeO_3$ reactivity was also ascribed to iron redox capacity and to the coexistence of the main Fe^{4+} species together with the Fe^{3+} ones, in association with the structure and the easy formation of oxygen vacancies [13].

Moreover, regarding the specific activity of strontium ferrate in pollutants removal, Leiw et al. [12] described a particular case, proposing a predominant role of superoxide anion radicals

by studying the production of ROS (reactive oxygen species as hydroxyl radical, superoxide anion radical and singlet oxygen) in the dark. Nevertheless, no investigation about the correlations between temperature, light and catalytic performances is present in the literature.

It is already known that a suitable amount of Ce^{4+} doping in A-site of $SrFeO_3$ (used as electro-catalyst) allows the stabilization of the Fe^{4+}–Fe^{3+} couple [5]. Since Ce^{4+} ions generate an extra-positive charge in A-site, compared to the divalent Sr, a compensation is required to reach the electroneutrality which can be provided, for example, by the decrease in valence of B-site cations (electronic compensation). Another important effect of Ce addition is the stabilization of the octahedral Fe^{3+} site and the cubic environment, which is usually more efficient than other structures in enhancing ionic and electronic conduction [4,13], *i.e.* by favouring the interaction between the redox couples Ce^{4+}–Ce^{3+} and Fe^{4+}–Fe^{3+} connected in the solid solution by oxygen bridges. Therefore, it is expected that a Ce-doped $SrFeO_3$ is able to enhance the interaction with oxygen species during a catalytic reaction.

Previous studies demonstrated that Ce-doped $SrFeO_3$ redox properties are improved by Ce doping [5] and recent results on $Sr_{0.85}Ce_{0.15}FeO_{3-}$ as H_2O_2 sensor [13] confirmed a positive role of Ce in oxidation reactions. Therefore, in this work, $Sr_{0.85}Ce_{0.15}FeO_{3-}$ was synthesized and characterized in terms of physical-chemical features and applied to remove two charged dyes (Orange II and Rhodamine B) from aqueous solution. Moreover, the correla- tion between temperature-activation, light-activation and catalytic performance of $Sr_{0.85}Ce_{0.15}FeO_{3-}$ was investigated in details for the first time.

2. Experimental

2.1. Perovskite oxide synthesis

$Sr_{0.85}Ce_{0.15}FeO_{3-}$ (SF) was synthesized by solution combustion synthesis according to a procedure already used in previous papers [14,15]. All the reagents were bought from Sigma Aldrich and were used without further purification.

$Sr(NO_3)_2$ (1.8049 gr), $Ce(NO_3)_3{\cdot}6H_2O$ (0.6535 gr) and $Fe(NO_3)_3\,9H_2O$ (4.0539 gr) were dissolved in 200 mL of dis- tilled water. Proper amounts of citric acid (the combustion fuel), reducer-to-oxidizer ratio ( ) and pH regulators (NH_4NO_3 and NH_4OH, respectively) were added in order to reach these conditions: citric acid/metal nitrates molar ratio = 2; = 1; pH = 6. The solution was placed in a 1 L stainless steel beaker in contact with a hot plate and the water was left to evaporate at 80 °C under continuous magnetic stirring until a sticky gel was obtained. The temperature control was ensured by means of a thermocouple inserted in the precursor's mixture. The temperature was then raised up to 220 °C (effective temperature inside the beaker) in order to decompose the gel by self-ignition. From this procedure, about 2 g of $Sr_{0.85}Ce_{0.15}FeO_{3-}$ were obtained after final calcination at 1000 °C for 5 h.

2.2. Perovskite oxide characterization

The temperature–time profile of the reaction medium was recorded during the combustion process by means of a K-type thermocouple (1.5 mm in diameter) coupled with a data logger (PICO technology) with a sampling velocity of 20 bit per second and a computer with Picolog software.

X-ray diffraction (XRD) measurements were carried out ona Bruker-Siemens D5000 X-ray powder diffractometer equipped with a Kristalloflex 760 X-ray generator and with a curved graphite monochromator using Cu Ka radiation (40 kV/30 mA). The 2θ step size was 0.03 and the integration time was 3 s per step. The diffraction patterns were analysed by Rietveld refinement using the GSAS package [16,17], while the Findit ICSD database was used for obtaining the structural data of the reference phases ($Sr_{0.85}Ce_{0.15}FeO_3$ #249012 and CeO_2 #290464). Chebyshev polynomial functions were chosen for the background and for the peak profile fitting. Lattice constants, Debye Waller factors, microstrain and full width at half maximum (FWHM) were considered as variable parameters in the structure refinement. From fitting results, the structural parameters of the investigated compound, *i.e.*: phase composition and the relative cell edge lengths, were obtained. Moreover, an estimation of the crystal size values was carried out by Scherrer equation in agreement with the GSAS package procedure. A standard deviation of 0.003 Å for the refined cell parameters was calculated in the experimental conditions used in this work. The obtained Debye Waller factors for the perovskite-type phase are in good agree- ment with the literature. The agreement factors, the goodness of fit(x^2) and the reliability factors (R factors, expressed as percentage values), whose detailed definitions are given elsewhere in the literature, are reported in the text as quality indicators for the Rietveld fitting [18]. Such agreement factors are only statistically defined parameters and they are generally acceptable when x^2 is close to 1 and R factors are lower than 10%, but in some cases high instrumental resolution and larger number of counts might increase the R factors, without necessarily resulting in a lower quality of the model [19].

In order to remove and quantify the unburned carbon, the powder was suspended in MilliQ^{TM} water (500 mg L^{-1}) and stirred for 2 h. The suspension was centrifuged at 7000 rpm for 15 min and the surnatant was separated for the quantification of the total organic carbon (TOC). The instrument used was a Shimadzu TOC-V CSH, based on catalytic oxidation of carbon on supported Pt at 680 °C. Produced CO_2 was revealed by a non-dispersive infrared detector (NDIR).

Specific surface area and porosity were determined by studying the gas-volumetric N_2 uptake at N_2 boiling point (–196 °C) using an ASAP2020 gas-volumetric apparatus by Micromeritics. BET model [20] was applied for specific surface area determination and BJH model [21] was applied to the desorption branch of the isotherms and used for mesoporosity characterization. Sample analyses were performed after outgassing the materials in vacuum (residual pressure ~10^{-2} mbar) for several hours at 300 °C in order to reach a good surface cleaning.

Zeta potential measurements were performed on a Zetasizer Nano ZS Malvern Instrument. The zeta potential values were measured using principles of laser Doppler velocitometry and phase analysis light scattering (M3-PALS technique). All the suspensions were prepared using 3 mg of powder and 12 mL of ultrapure water, obtained from a Millipore MilliQ^{TM} system (TOC = 6 ppb).

Scanning electron microscopy (SEM) analyses were carried out using a ZEISS EVO 50 XVP with LaB_6 source, equipped with detectors for secondary electrons collection and EDS probe for elemental analyses. Samples were covered with a gold layer of ~15 nm of thickness before the analysis to avoid any charging effect (Bal-tec SCD050 sputter coater) due to their insulating properties.

High-Resolution Transmission Electron Microscopy (HRTEM) was performed using a JEOL JEM 3010UHR (300 kV) instrument equipped with a single crystal LaB_6 filament. The sample was dry-deposited on Cu "holey" carbon grids (200 mesh) for the analysis.

2.3. (Photo)catalytic tests

For the photocatalytic tests, aqueous suspensions of SF (750 mg L^{-1}) and substrate, Orange II (sodium salt, >85%) orRhodamine B (>95%) 10 mg L^{-1}, were prepared with Milli-Q^{TM} ultrapure water and stirred for 30 min in order to homogenize the

suspension before irradiation. The photodegradation trials were performed by irradiating the suspensions (5 mL) in closed Pyrex® cells under continuous stirring. Solar radiation was simulated in Solarbox (CO.FO. Megra, Mi), a system equipped with Xenon lamp (1500 W) and cut-off filter for wavelengths below 340 nm. For the sake of comparison, dark tests were carried out, by stirring the suspensions in Solarbox, covering the closed Pyrex® cells with aluminium foils, thus taking into account only the temperature effects. Dark tests at room temperature were also conducted. After different times of irradiation/dark tests, the samples were filtered on PTFE membrane by using syringe Minisart® and Syringe Filters 0.45 μm. The dyes photobleaching was followed by a double-beam UV–vis spectrophotometer CARY 100 SCAN-VARIAN. A sample quartz cell of 1 cm path length was used and the spectra were recorded in the range 200–700 nm. Quantification of dyes degradation *vs* time was performed at the wavelength of maximum absorbance of each dye (485 nm for Orange II and 555 nm for Rhodamine B).

Temperature effect on the Orange II degradation was studied by a UNICAM UV300 (Thermospectronic) double beam spectrophotometer equipped with a stirring system and a Peltier cell for temperature control, allowing the temperature variation inside the cuvette (from room temperature to 80 °C) and the spectra acquisition *in situ*. For each temperature chosen, the points were acquired for at least 6 h. The measurements were carried out taking into account the absorption of the suspension at 485 nm, interrupting the stirring to let the powder deposit and to avoid the scattering effect in the spectra. A kinetic study was conducted fitting the curves resulted from these tests with a first order decay, using the equation $y = A \times e^{(-k_{obs} \times t)} + y_0$.

All the results showed in the graphs for all the trials are reported as A/A_0 decay, namely the absorbance ratio between the dye solution of the suspension under consideration (which underwent the degradation) related to 10 mg L^{-1} dye.

The study of the reactive species was conducted by Electron Paramagnetic Resonance (EPR) in the presence of 5,5-dimethyl- 1-pyrroline-*N*-oxide (DMPO), 2,2,6,6-tetramethyl-4-piperidone hydrochloride (4- oxo-TMP), and 5-(diethoxyphosphoryl)-5-methyl-1-pyrroline-*N*-oxide (DEPMPO) as spin-trap [22,23]. EPR spectra were recorded at room temperature with a Bruker ESR 300E X-band spectrometer. The acquisition parameters were as follows: frequency = 9.78 GHz, microwave power = 5 mW, center field = 3470 G, sweep width = 80 G, receiver gain = 1×10^5, modulation amplitude = 0.41 G, conversion time = 40.96 ms. As previously reported [24,25], the experiments were carried out by adding the spin trap in the cell at the desired temperature or after 2 h irradiation in Solarbox both in light and in dark conditions; after 15 min of incubation in the same experimental conditions, an aliquot of sample was withdrawn in a capillary quartz tube and the EPR spectrum was immediately acquired.

Since hydroxyl radicals were detected in the system, 2-propanol (Fluka) was added in different concentrations (0.01 and 0.1 M) as $^{\cdot}OH$ scavenger during the experiment at 70 °C in the UV–vis thermostatic cell, to confirm the active role of this species in the catalytic reaction.

3. Results and discussion

3.1. SF synthesis and characterization

During the combustion synthesis of SF the temperature-time profile was recorded (Fig. 1) in order to obtain information about the kinetics of the combustion process. The combustion profile of SF corresponds to that expected for this kind of material prepared in this synthetic conditions [15]. The combustion reaction starts when the gel reaches 270 °C, subsequently the combustion process

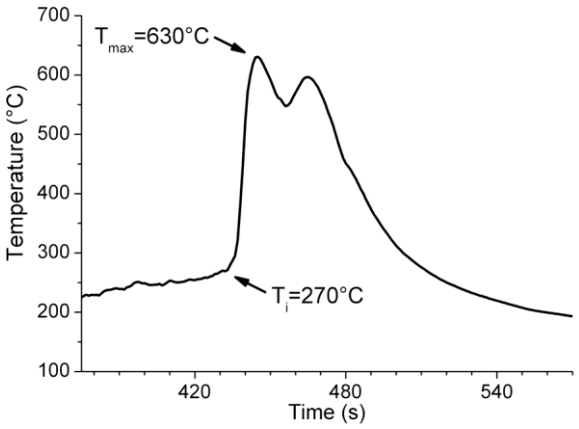

Fig 1. Temperature-time profile registered during the combustion synthesis of SF. T_i is the temperature at which the reaction started and T_{max} is the maximum temperature recorded during the synthesis.

takes place in 100 s reaching the highest temperature of 630 °C. The presence of a doubled peak in the temperature-time profile suggests the formation of different crystalline phases during the high-temperature combustion process [26].

According to previous studies regarding other mixed oxides prepared by SCS [15,27], the presence of unreacted organic precursors in the final material was expected. To confirm this hypothesis, the powder was washed with Milli-Q water for two hours under stirring and the washing water was analysed for TOC determination, revealing the presence of 0.84 mg L^{-1} of total organic carbon.

The removal of organic carbon can influence the morphological behaviour of the perovskite powder. Therefore, the textural properties were studied by nitrogen adsorption before and after the washing treatment, as reported in Fig. 2. Both the adsorption isotherms in Fig. 2a can be classified as IV type (IUPAC classification), typical of mesoporous powders. After washing, it is possible to observe an increase of the global amount of nitrogen adsorbed and of BET specific surface area and mesoporosity in terms of cumulative pore volume (Table in Fig. 2b). The pore size distribution in Fig. 2b indicates that a large amount of pores in the range 20–500 Å has become available to N_2 adsorption after washing and removal of entrapped unreacted precursors.

On the basis of these evidences, as prepared powders (unwashed) were not taken into account for further studies.

Results from the XRD analysis and Rietveld refinement of the calcined SF powder are shown in Fig. 3. Cell parameters are consistent with a typical $Sr_{1-x}Ce_xFeO_3$ phase with cubic *Pm-3 m* structure [4,5]. Matching between XRD patterns of the sample and the reference phase from the database (ICSD #249004) is good, as confirmed by the graphical fitting and by the values of the agreement factors ($x^2 = 1.48$; $R_p = 13.6\%$; $wR_p = 17.4\%$; $R_F^2 = 9.3$). Other signals are observed in the pattern (some of them are evidenced by a cross), due to a small amount of segregated CeO_2, whose solubility in $SrFeO_3$ is limited at about 14% mol of Ce [5,28].

EDS analysis shows 0.15:1 as Ce/Fe ratio, confirming the presence of cerium in the synthesized product and the total amount expected from the synthesis stoichiometry. The EDS elemental mapping evidences the perfect homogeneity of the sample. Nevertheless, the diffractogram reported in Fig. 3 shows the presence of segregated cerium oxide, whose amount, determined by means of Rietveld refinement as 2 mol%, needs to be excluded from the total amount observed by EDS to obtain the correct amount of cerium in the doped SF, which corresponds to 13 mol%.

The morphology of the washed sample, studied by SEM anal- ysis (Fig. 4), indicates that SF was formed in aggregates with very different shapes, from lengthened to laminar flakes, suggest-

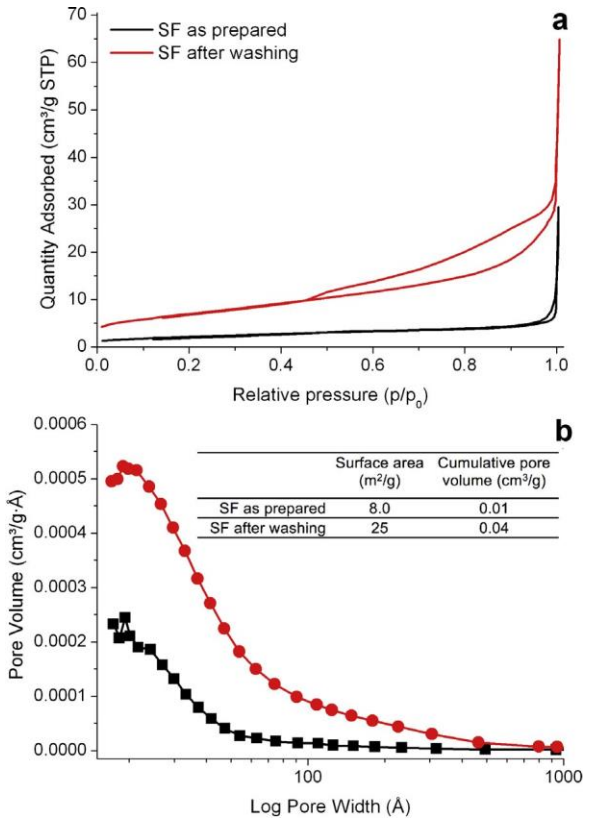

Fig. 2. (a) N_2 adsorption isotherms and (b) pore size distribution curves for the strontium ferrate as prepared (line and squares in black) and after washing (lines and circles in red). The table shows BET specific surface area and BJH total porosity values. (For interpretation of the references to colour in this figure legend, the reader is referred to the web version of this article.)

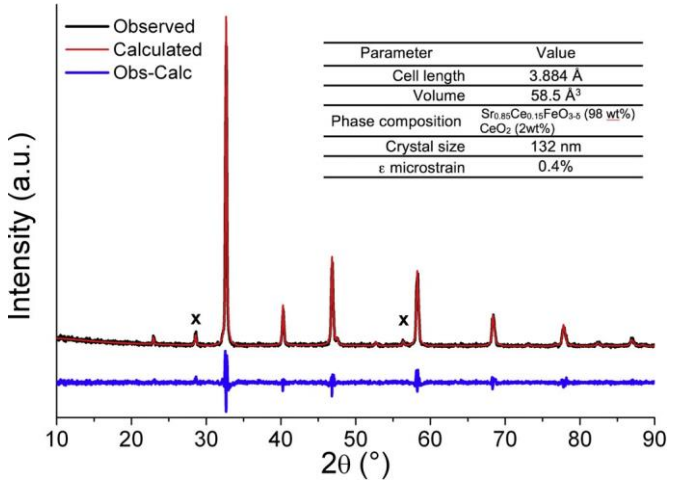

Fig. 3. Graphical Rietveld refinement and main structural parameters (in the insert table) related to calcined SF. Signals ascribable to CeO_2 are evidenced with a cross. Indication *Obs-Calc* indicates the discrepancy between observed and calculated pattern.

ing different growth processes during synthesis. Laminar flakes (as those evidenced in the inset of the figure) seem to be made of aggregated irregular sub-micrometric spherical-like particles, which form interparticle pores, whereas the needle-like particles appear dense and not porous. It cannot be ruled out that elon- gated parts are related to strontium carbonate impurities that can be formed after the prolonged time exposure of the perovskite to the carbon dioxide in the atmosphere.

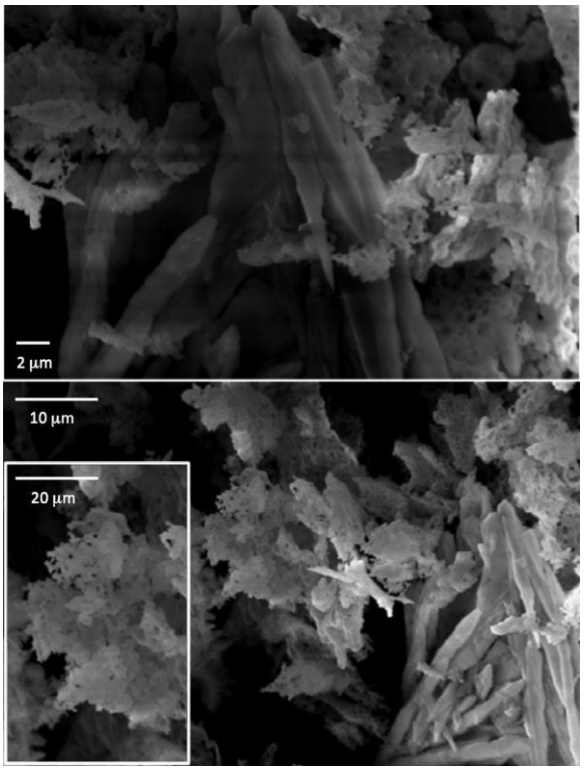

Fig. 4. SEM micrographs of SF at different magnifications. In the inset an enlarged detail of the underlying micrograph.

TEM images are shown in Fig. 5. The presence of elongated and roundish aggregated particles is confirmed as well at the nanometric scale. The size of the particles is quite variable. For what concerns the analysis of the fringe patterns, the system is extensively crystalline. Unfortunately, the main perovskite phase under examination, $Sr_{0.85}Ce_{0.15}FeO_3$, is not indexed in the databases, nevertheless it can be compared with an undoped cubic strontium ferrate. The value of d_{hkl} = 2.73 Å belongs to this phase (plane (110), reference pattern #00-040-0905). However, the same value can be also attributed to some cubic CeO_2 (plane (200), reference pattern #00-034-0394). Moreover, beyond the cerium oxide presence, it is possible to ascribe the values 3.30 and 2.52 Å to a tetragonal SrO_2 phase (reference pattern #00-001-1113), probably derived from A-site imbalance due to ceria segregation. Finally, several values (2.89, 2.50, 2.38, and 2.30 Å) can be assigned to planes (102), (202), (311) and (212) of $SrCeO_3$ (reference code #01-082-2427), indicating the presence of other crystalline phases formed in the final material.

Zeta potential values of the SF suspension in water were measured in a pH range 5–9.5 (Fig. 6). It was possible to determine that in acid environment the surface of SF is positively charged, with a starting value of 23.1±2.7 mV at pH 5, whereas at basic pH it is negative. At pH 9.5, namely the working pH reached in the presence of dye during the catalytic experiments described in the next sections, the observed value was -5.8 ± 0.7 mV.

3.2. SF activity in dyes degradation

SF ability as photocatalyst was tested in the degradation of two different dyes, Orange II and Rhodamine B (Fig. 7), by irradiation in Solarbox. Control experiments in the dark as well as adsorption tests were also performed. The concentrations of SF and dyes were chosen on the basis of previously published papers concerning the degradation of pollutants by undoped $SrFeO_3$ [7,9–11] and $LaFeO_3$

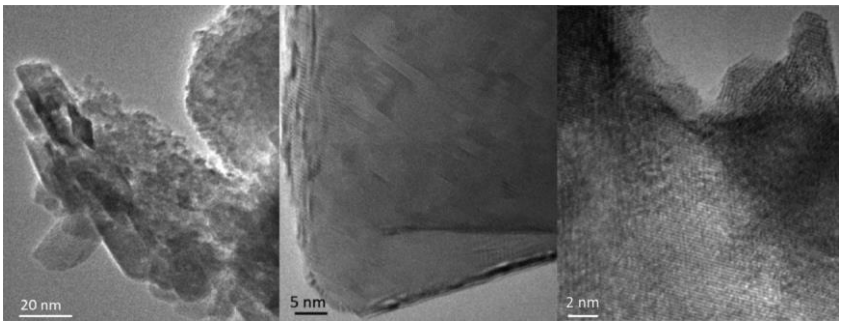

Fig. 5. HR-TEM micrographs of SF at different magnifications.

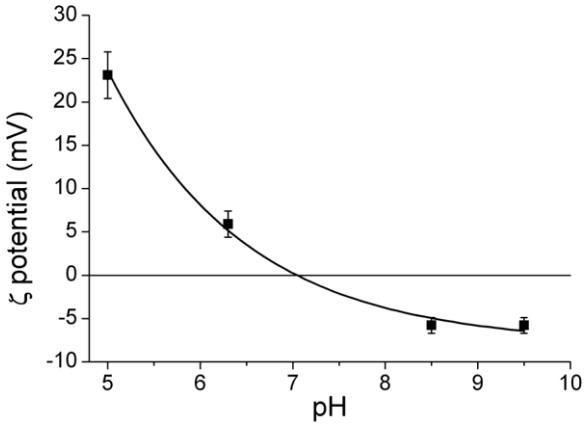

Fig. 6. ζ potential of SF suspensions in water measured at different pH values.

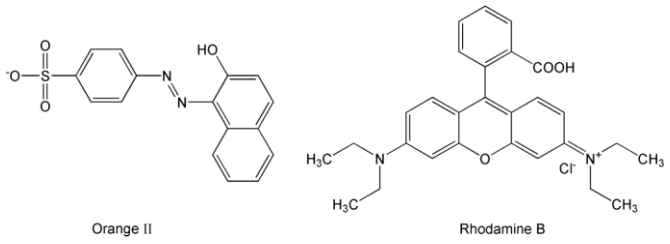

Fig. 7. Chemical structures of Orange II and Rhodamine B.

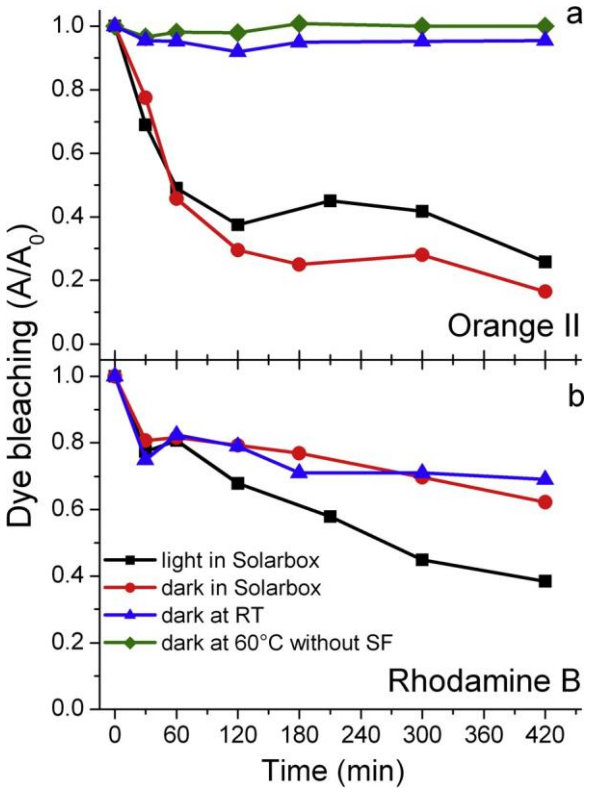

Fig. 8. Dye bleaching vs. time for 10 mg L^{-1} solutions of Orange II (a) and Rhodamine B (b) in the presence of 750 mg L^{-1} SF. Experimental data were collected under direct irradiation in Solarbox (black squares) and in dark condition in Solarbox (red circles) or at RT (blue triangles). In the case of Orange II, dye bleaching was also studied at 60 °C without SF (green diamonds). (For interpretation of the references to colour in this figure legend, the reader is referred to the web version of this article.)

[15]. These measurements revealed unexpected properties of SF, which will be described in detail in the next paragraphs.

A preliminary test was done in order to assess the Orange II adsorption on SF at room temperature (RT=25 °C); an adsorption of 5% was evidenced throughout the experiment duration (7 h) and it is indicated by blue triangles in Fig. 8a, referring to the ini- tial Orange II solution concentration (10 mg L^{-1}). The same figure reports the Orange II bleaching by SF photocatalyst under light irradiation (black squares) as well as in the dark (red circles); both experiments were performed in Solarbox, where the average T is 60 °C; dark experiments were performed by wrapping with aluminium foil the cell containing SF and Orange II (see Experimental). Surprisingly a relevant dye bleaching, comparable to the light-induced one, was observed also in the dark, whereas Orange II degradation is substantially negligible at 60 °C in the absence of SF (green diamonds).

A desorption procedure was then adopted to confirm the effectiveness of the dye degradation instead of the simply adsorption on the SF powder. Acetonitrile was used to wash the suspensions after the experiments with and without irradiation for 7 h in order to evidence the presence of unreacted dye. In both cases, the results allowed to exclude relevant adsorption phenomena on SF surface, if compared to the degradation ones. Concerning the dye bleaching occurred in the dark, a crucial role of the temperature rise to 60 °C can be hypothesized, since no bleaching was observed for Orange II solutions stored at RT, both with and without SF.

In order to verify the behaviour of SF with another substrate, the same tests in Solarbox were carried out with Rhodamine B. Surprisingly, significantly different results were obtained (Fig. 8b). In this case, lower light-induced abatement levels were achieved (black squares) and no temperature-based effect was observed. The adsorption measured after the initial stirring, necessary for the homogenization of the system, before irradiation, was ~30% (blue triangles) referring it to a solution 10 mg L^{-1} Rhodamine B as standard. Adsorption kinetic at RT was very similar to that resulted in dark experiments in Solarbox (red circles), indicating, in both conditions, a certain affinity of the dye with the SF surface (acetonitrile washing confirms the adsorption phenomena since unreacted dye

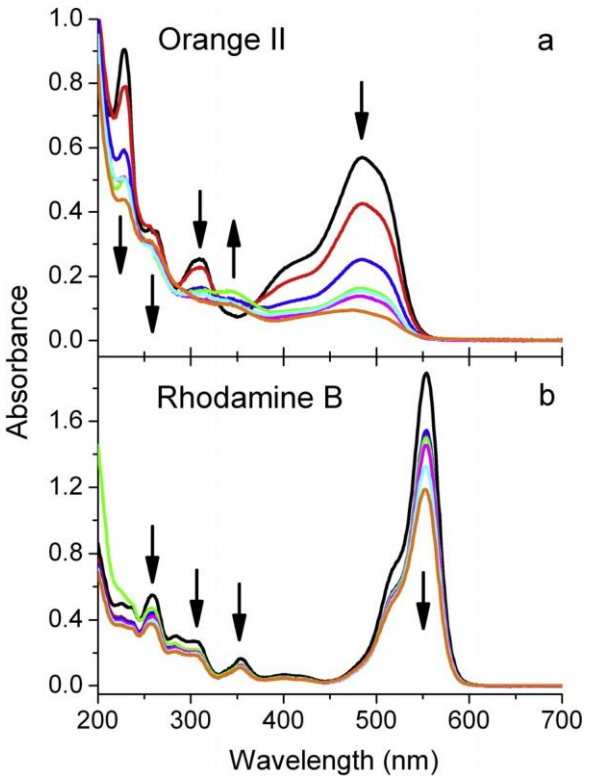

Fig. 9. Spectra of Orange II (a) and Rhodamine B (b) at different times during dark experiments in Solarbox. Arrows indicate the behaviour of the main absorption bands during the experiments. (For interpretation of the references to colour in this figure legend, the reader is referred to the web version of this article.)

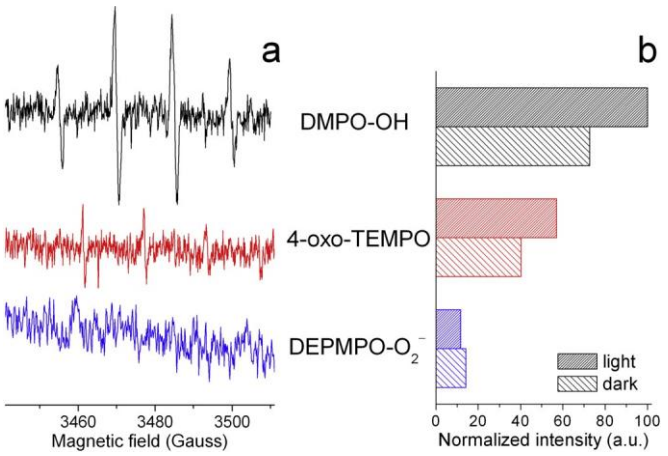

Fig. 10. (a) EPR spectra of different adducts spin-trap/ROS obtained in the presence of SF after 2 h in Solarbox. (b) Comparison of the relative normalized intensity of the different adducts obtained after treatment in Solarbox with exposition to the light and in the dark.

was recovered from the SF material). This affinity could be ascribed to an electrostatic interaction between the cationic Rhodamine B and the negatively charged SF surface in the operating conditions, as shown by ζ-potential value.

The better performances observed under irradiation could be due to a direct oxidation of the adsorbed Rhodamine B by the surface trapped hole generated upon SF irradiation. By comparing the behaviour of the two dyes, it seems that a correlation exists between the dye adsorption on the SF surface and the absence of thermal degradation.

As for the degradation mechanism, the UV–vis spectra of the dyes recorded after irradiation (not reported for the sake of brevity) show the progressive reduction of the main absorption peaks. In dark conditions, Orange II spectra (Fig. 9a) show a similar trend with respect to corresponding experiments upon light, with the decrease of the main absorption peaks at 485, 310, 261 and 228 nm and the contemporary appearance of an absorption band with a maximum at about 350 nm, amenable to intermediates production. This kind of behaviour was previously observed in the literature and attributed to the breaking of the diazo bond of Orange II with formation of a mixture of primary intermediate compounds such as 1,2-dihydroxynaphthalene, 4-hydroxybenzenesulfonate and 4-nitrosobenzenesulfonate [29,30].

In the case of Rhodamine B tests, only a progressive decreasing of the dye absorbance was observed (Fig. 9b), suggesting that a simple adsorption phenomenon is occurring in these conditions.

3.3. EPR studies on ROS generation

A previous study on the dark degradation of Bisphenol A and Acid Orange 8 by $SrFeO_3$ perovskite [12] reports on the possi-ble formation of $O_2^{\bullet -}$ as responsible for the degradation, whereas less relevant role was hypothesized for singlet oxygen and $^{\bullet}OH$ radicals. Therefore, in order to clarify the role of the ROS in the reaction mechanism of $Sr_{0.85}Ce_{0.15}FeO_{3-}$ perovskite, EPR spin-trap approach was applied by using three different spin-trap molecules: 4-oxo-TMP for singlet oxygen, DMPO for hydroxyl radical and superoxide, DEPMPO, specific for superoxide anion radical.

EPR spectra obtained after addition of a spin-trap to a SF suspension in water (750 mg L^{-1}), previously irradiated for 2 h in Solarbox, were reported in Fig. 10a. The typical 1:2:2:1 spec- trum of DMPO OH radical species, and the 1:1:1 pattern ofthe 4-oxo-TEMPO (4-oxo-2,2,6,6-tetramethyl-1-piperidine-N-oxyl radical) are easily observable in the figure, whereas the adduct of DEPMPO with superoxide radical anion is quite weak.

The same experiments were also performed in the dark, covering the cell in solarbox as described above. The results obtained are similar, but the concentrations of the three ROS-adducts are quite different, as can be observed in Fig. 10b where the relative normalized intensities of the three species observed after treatment in Solarbox with light or in the dark are shown. The very low amount of superoxide trapped in these experiments is also in agreement with the absence of any signal attributable to this species in the experiment with DMPO.

The same results were obtained when these experiments were performed towards SF suspensions in Orange II or Rhodamine B solution, whereas no signal was recorded at RT and when dyes solutions underwent thermal or irradiation treatments in the absence of SF.

In general, the same kind of ROS were generated in both the systems examined, but the degradation efficiency for Orange II was considerably higher than in Rhodamine B case. In the literature superoxide anion radical is supposed to be the main species able to degrade this cationic dye [31,32], thus a possible explanation of the discrepancy of SF behaviour towards Rhodamine B degradation could be imputable to the very limited production of $O_2^{\bullet -}$ in favour of preponderant generation of hydroxyl radical.

3.4. Studies on Orange II degradation kinetic

The reaction mechanism does not seem to be only correlated with the irradiation, but, as reported above, the effect of the temperature seems to be important. Therefore, the dependence of the SF behaviour on the temperature was ascertained by performing a systematic study of Orange II degradation in the presence of SF suspension and in the range 55–80 °C; experiments were carried out

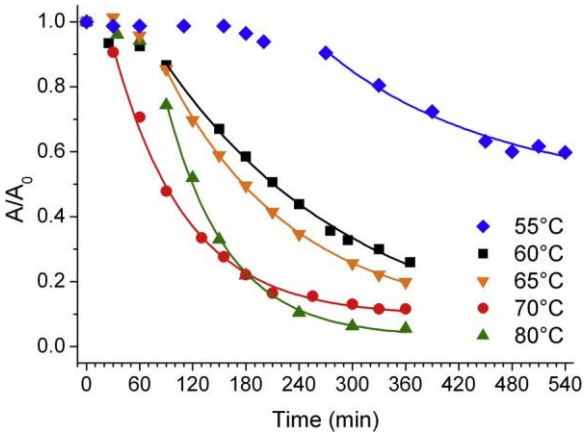

Fig. 11. Degradation of a 10 mg L^{-1} Orange II solution in the presence of 750 mg L^{-1} SF at different temperatures.

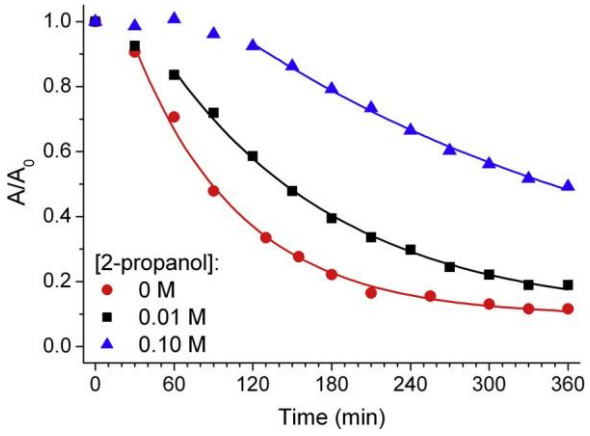

Fig. 12. Degradation of a 10 mg L^{-1} Orange II solution in the presence of 750 mg L^{-1} SF at 70 °C in the absence (red circles, same data of Fig. 11) and in the presence of 2-propanol 0.01 M (black squares) and 0.1 M (blue triangles). (For interpretation of the references to colour in this figure legend, the reader is referred to the web version of this article.)

Table 1
First order k_{obs} values (min^{-1}) at different temperatures calculated from the data reported in Fig. 11.

Temperature (°C)	k_{obs} (min^{-1})
55	0.00419 ± 0.00240
60	0.00465 ± 0.00053
65	0.00698 ± 0.00024
70	0.01221 ± 0.00067
80	0.01441 ± 0.00085

in a thermostatic cell and the progressive disappearing of Orange II was followed by recording the UV–vis spectrum of the solution (see Section 2.3 for the procedure).

In Fig. 11, Orange II degradation curves registered at different temperatures in presence of SF are reported: increasing T, abatement rate and degree go through a gain. If considering only the process after the activation time, the curves fit a first-order kinetic law and, consequently, the first order k_{obs} values enhance proportionally with the temperature (Table 1). These data confirm the previous speculations about the influence of the temperature in SF photo-catalytic experiments.

Arrhenius plot, reporting ln k_{obs} *vs* 1/T, allows to obtain the activation energy for the Orange II abatement process on SF which corresponds to 51.5 kJ/mol with an A value (pre-exponential term, extrapolated on the y-axis as ln A) of 6.73 $\times 10^5$.

Aiming to deepen the knowledge about ROS role and to prove the $^{\bullet}OH$ activity, further experiments were performed by following the Orange II bleaching, at 70 °C, in the presence of 2-propanol ($^{\bullet}OH$ scavenging agent), at 0.01 and 0.1 M. As expected, in Fig. 12 it is evidenced that the 2-propanol addition severely decreases the rate of dye abatement. Thus, the k_{obs} value changes from 0.01221 min^{-1} to 0.00742 min^{-1} (at 0.01 M) and 0.00301 min^{-1} (at 0.1 M). This result demonstrates the crucial role of hydroxyl radicals in the Orange II abatement from SF.

4. Conclusions

A $Sr_{0.85}Ce_{0.15}FeO_{3-}$ (SF) perovskite-type oxide was synthesized by solution combustion synthesis, deeply characterized and tested as catalyst for Orange II and Rhodamine B degradation. For the first time, to the best of our knowledge, the behaviour of this material was revisited in terms of action mechanism, as its role was not yet assessed neither fully understood. Actually, this material showed both photocatalytic activity (under a simulated solar light) and a temperature-dependent catalytic behaviour activated by low temperatures in a very narrow temperature range, between 55 and 80 °C. SF performed efficiently in Orange II abatement and reaction rate constant was enhanced by means of temperature increase, due to a consequent increment of active hydroxyl radical production. Indeed, 95% degradation of Orange II was obtained at 80 °C, comparable with the results of Yang et al. [10] concerning the photodegradation of methylorange by $SrFeO_3$. For Rhodamine B, significantly lower levels of photobleaching together with a significant adsorption phenomenon were observed, without any correlation with the temperature.

In conclusion, it was found that excitation modes, generated ROS and catalyst surface/dyes interactions represent interconnected and determining parameters that can be finely regulated for tuning the activity and the selectivity in the substrate attack.

Furthermore, some conclusions about the mechanistic aspects of SF action can be also deduced by the experimental results:

a) SF induces the formation of hydroxyl radicals, both by irradiation and thermal activation;
b) Orange II degradation strictly depends on hydroxyl radicals generation, as revealed by the experiments in the presence of 2-propanol as scavenger;
c) Rhodamine B is less affected by hydroxyl radicals action, its degradation is probably favoured by the presence of a small amount of superoxide radicals, in agreement with the literature [31,32].
d) Adsorption is influenced by electrostatic interaction between charged surface of SF and dyes. The higher adsorption of Rhodamine B (positively charged) with respect to Orange II (negatively charged) is in agreement with the zeta potential measurements showing that SF is negatively charged at the experimental pH.

Finally, this work is a useful starting point to develop new strategies that evidence the action mechanism of materials and exploit them in pollutant abatement.

Acknowledgements

The scientific activities described in this paper belong to project MAT4TREAT: it has received funding from the European Union's Horizon 2020 research and innovation program under the Marie Skłodowska-Curie grant agreement no. 645551. Compagnia di San Paolo and University of Torino are gratefully acknowledgedfor funding Project Torino call2014 L2 126 through "Bando per il

finanziamento di progetti di ricerca di Ateneo–anno 2014" (Project acronym: Microbusters). The authors thank Dr. Francesco Giordano and Dr. Debora Fabbri for the XRD and TOC measurements, Dr. Roberto Nisticò and Dr. Maria Carmen Valsania for SEM and HRTEM analyses. Furthermore, Prof. Vittorio Boffa (Aalborg Univer- sity, Denmark) is acknowledged for making available Z-potential equipment.

References

[1] G. Wu, P. Li, D. Xu, B. Luo, Y. Hong, W. Shi, C. Liu, Hydrothermal synthesis and visible-light-driven photocatalytic degradation for tetracycline of Mn-doped $SrTiO_3$ nanocubes, Appl. Surf. Sci. 333 (2015) 39–47, http://dx.doi.org/10.1016/j.apsusc.2015.02.008.

[2] K. Yu, C. Zhang, Y. Chang, Y. Feng, Z. Yang, T. Yang, L.L. Lou, S. Liu, Novel three-dimensionally ordered macroporous $SrTiO_3$ photocatalysts with remarkably enhanced hydrogen production performance, Appl. Catal. B Environ. 200 (2017) 514–520, http://dx.doi.org/10.1016/j.apcatb.2016.07.049.

[3] W. Chen, H. Liu, X. Li, S. Liu, L. Gao, L. Mao, Z. Fan, W. Shangguan, W. Fang, Y. Liu, Polymerizable complex synthesis of $SrTiO_3$:(Cr/Ta) photocatalysts to improve photocatalytic water splitting activity under visible light, Appl. Catal. B Environ. 192 (2016) 145–151, http://dx.doi.org/10.1016/j.apcatb.2016.03.057.

[4] N.E. Trofimenko, H. Ullmann, Oxygen stoichiometry and mixed ionic-electronic conductivity of $Sr_{1-a}Ce_aFe_{1-b}Co_bO_{3-x}$ perovskite-type oxides, J. Eur. Ceram. Soc. 20 (2000) 1241–1250, http://dx.doi.org/10.1016/S0955-2219(99)00292-7.

[5] F. Deganello, L.F. Liotta, A. Longo, M.P. Casaletto, M. Scopelliti, Cerium effect on the phase structure, phase stability and redox properties of Ce-doped strontium ferrates, J. Solid State Chem. 179 (2006) 3406–3419, http://dx.doi.org/10.1016/j.jssc.2006.06.027.

[6] H. Falcón, J.A. Barbero, J.A. Alonso, M.J. Martínez-Lope, J.L.G. Fierro, $SrFeO_{3-}$ perovskite oxides: chemical features and performance for methane combustion, Chem. Mater. 14 (2002) 2325–2333, http://dx.doi.org/10.1021/cm011292l.

[7] C. Srilakshmi, R. Saraf, C. Shivakumara, Effective degradation of aqueous nitrobenzene using the $SrFeO_{3-}$ photocatalyst under UV illumination and its kinetics and mechanistic studies, Ind. Eng. Chem. Res. 54 (2015) 7800–7810, http://dx.doi.org/10.1021/acs.iecr.5b01474.

[8] M.V. Patrakeev, I.A. Leonidov, V.L. Kozhevnikov, V.V. Kharton, Ion-electron transport in strontium ferrites: relationships with structural features and stability, Solid State Sci. 6 (2004) 907–913, http://dx.doi.org/10.1016/j.solidstatesciences.2004.05.002.

[9] M. Ghaffari, P.Y. Tan, M.E. Oruc, O.K. Tan, M.S. Tse, M. Shannon, Effect of ball milling on the characteristics of nano structure $SrFeO_3$ powder for photocatalytic degradation of methylene blue under visible light irradiation and its reaction kinetics, Catal. Today. 161 (2011) 70–77, http://dx.doi.org/10.1016/j.cattod.2010.11.031.

[10] Y. Yang, Z. Cao, Y. Jiang, L. Liu, Y. Sun, Photoinduced structural transformation of $SrFeO_3$ and $Ca_2Fe_2O_5$ during photodegradation of methyl orange, Mater. Sci. Eng. B Solid State Mater. Adv. Technol. 132 (2006) 311–314, http://dx.doi.org/10.1016/j.mseb.2006.03.031.

[11] L. Jia, T. Ding, Q. Li, Y. Tang, Study of photocatalytic performance of $SrFeO_{3-x}$ by ultrasonic radiation, Catal. Commun. 8 (2007) 963–966, http://dx.doi.org/10.1016/j.catcom.2006.08.026.

[12] M.Y. Leiw, G.H. Guai, X. Wang, M.S. Tse, C.M. Ng, O.K. Tan, Dark ambient degradation of Bisphenol A and Acid Orange 8 as organic pollutants by perovskite $SrFeO_{3-}$ metal oxide, J. Hazard. Mater. 260 (2013) 1–8, http://dx.doi.org/10.1016/j.jhazmat.2013.04.031.

[13] F. Deganello, L.F. Liotta, S.G. Leonardi, G. Neri, Electrochemical properties of Ce-doped $SrFeO_3$ perovskites-modified electrodes towards hydrogen peroxide oxidation, Electrochim. Acta 190 (2016) 939–947, http://dx.doi.org/10.1016/j.electacta.2015.12.101.

[14] F. Deganello, G. Marcì, G. Deganello, Citrate-nitrate auto-combustion synthesis of perovskite-type nanopowders: a systematic approach, J. Eur. Ceram. Soc. 29 (2009) 439–450, http://dx.doi.org/10.1016/j.jeurceramsoc.2008.06.012.

[15] F. Deganello, M.L. Tummino, C. Calabrese, M.L. Testa, P. Avetta, D. Fabbri, A.B. Prevot, E. Montoneri, G. Magnacca, A new, sustainable $LaFeO_3$ material prepared from biowaste-sourced soluble substances, New J. Chem. 39 (2015) 877–885, http://dx.doi.org/10.1039/C4NJ01279H.

[16] A.C. Larson, R.B. Von Dreele, General Structure Analysis System (GSAS), Los Alamos National Laboratory Report LAUR 86-748, 2004.

[17] B.H. Toby, EXPGUI, a graphical user interface for GSAS, J. Appl. Crystallogr. 34 (2001) 210–213, http://dx.doi.org/10.1107/S0021889801002242.

[18] L.B. McCusker, R.B. Von Dreele, D.E. Cox, D. Louër, P. Scardi, Rietveld refinement guidelines, J. Appl. Crystallogr. 32 (1999) 36–50, http://dx.doi.org/10.1107/S0021889898009856.

[19] B.H. Toby, R factors in Rietveld analysis: how good is good enough? Powder Diffr. 21 (2006) 67–70, http://dx.doi.org/10.1154/1.2179804.

[20] S. Brunauer, P.H. Emmett, E. Teller, Adsorption of gases in multimolecular layers, J. Am. Chem. Soc. 60 (1938) 309–319, http://dx.doi.org/10.1021/ja01269a023.

[21] E.P. Barrett, L.G. Joyner, P.P. Halenda, The determination of pore volume and area distributions in porous substances. I. Computations from nitrogen isotherms, J. Am. Chem. Soc. 73 (1951) 373–380, http://dx.doi.org/10.1021/ja01145a126.

[22] S. Dikalov, J. Jiang, R.P. Mason, Characterization of the high-resolution ESR spectra of superoxide radical adducts of 5-(diethoxyphosphoryl)-5-methyl-1-pyrroline N-oxide (DEPMPO) and 5,5-dimethyl-1-pyrroline N-oxide (DMPO). Analysis of conformational exchange, Free Radic. Res. 39 (2005) 825–836, http://dx.doi.org/10.1080/10715760500155688.

[23] J. Moan, E. Wold, Detection of singlet oxygen production by ESR, Nature 279 (1979) 450–451, http://dx.doi.org/10.1038/279450a0.

[24] A. Bianco Prevot, P. Avetta, D. Fabbri, E. Laurenti, T. Marchis, D.G. Perrone, E. Montoneri, V. Boffa, Waste-derived bioorganic substances for light-induced generation of reactive oxygenated species, ChemSusChem 4 (2011) 85–90, http://dx.doi.org/10.1002/cssc.201000237.

[25] P. Avetta, F. Bella, A. Bianco Prevot, E. Laurenti, E. Montoneri, A. Arques, L. Carlos, Waste cleaning waste: photodegradation of monochlorophenols in the presence of waste-derived photosensitizer, ACS Sustain. Chem. Eng. 1 (2013) 1545–1550, http://dx.doi.org/10.1021/sc400294z.

[26] A. Varma, A.S. Mukasyan, A.S. Rogachev, K.V. Manukyan, Solution combustion synthesis of nanoscale materials, Chem. Rev. 116 (2016) 14493–14586, http://dx.doi.org/10.1021/acs.chemrev.6b00279.

[27] G. Magnacca, G. Spezzati, F. Deganello, M.L. Testa, A new in situ methodology for the quantification of the oxygen storage potential in perovskite-type materials, RSC Adv. 3 (2013) 26352–26360, http://dx.doi.org/10.1039/c3ra44930k.

[28] H. Choi, A. Fuller, J. Davis, C. Wielgus, U.S. Ozkan, Ce-doped strontium cobalt ferrite perovskites as cathode catalysts for solid oxide fuel cells: effect of dopant concentration, Appl. Catal. B Environ. 127 (2012) 336–341, http://dx.doi.org/10.1016/j.apcatb.2012.08.027.

[29] A. Zhang, L. Fang, J. Wang, W. Liu, Enzymatic decolorization of Orange II: optimization by response surface methodology and pathway, Environ. Prog. Sustain. Energy 32 (2013) 294–301, http://dx.doi.org/10.1002/ep.11628.

[30] P. Calza, D. Zacchigna, E. Laurenti, Degradation of orange dyes and carbamazepine by soybean peroxidase immobilized on silica monoliths and titanium dioxide, Environ. Sci. Pollut. Res. 23 (2016) 23742–23749, http://dx.doi.org/10.1007/s11356-016-7399-1.

[31] S. Liu, K. Yin, W. Ren, B. Cheng, J. Yu, Tandem photocatalytic oxidation of Rhodamine B over surface fluorinated bismuth vanadate crystals, J. Mater. Chem. 22 (2012) 17759–17767, http://dx.doi.org/10.1039/c2jm33337f.

[32] H. Fu, C. Pan, W. Yao, Y. Zhu, Visible-light-induced degradation of rhodamine B by nanosized Bi_2WO_6, J. Phys. Chem. B 109 (2005) 22432–22439, http://dx.doi.org/10.1021/jp052995j.